RAYLEIGH NUMBER RAMPS CAUSE MOVING CONVECTION PATTERNS

I. Rehberg and H. Riecke

Physikalisches Institut, Universität Bayreuth,
Postfach 101251, D-8580 Bayreuth, Fed. Rep. of Germany

Summary

In this paper the induction of moving (drifting) patterns by wavelength selection is investigated. In the first part the theory for selection by ramps (i.e. control parameters which vary slowly in space) and the resulting motion is reviewed. Particular emphasis is put on qualitative features which should appear in most pattern forming systems if their dynamics is not derived from a minimizing potential. For experimental relevance of this theory the influence of imperfections (pinning centers) has to be taken into account. In the second part the experimental investigation of moving convection patterns in a convection cell with ramps is presented. In agreement with the theoretical predictions it is found that

— Drifting patterns are observable,
— Due to the pinning centers drifting starts at a value R_m of the control parameter well above the onset of convection R_c,
— The drift velocity approaches zero at R_m.

Introduction

In pattern-forming systems like Rayleigh-Benard convection and Taylor-Couette flow the wavelength of the patterns is not unique, the patterns are stable within a certain band. The related question of a "preferred" wavelength cannot be answered in the usual experimental set-ups as the distance between the two ends fixes the wavelength. In order to get rid of these ends one is led to the idea of a subcritical ramp /1/: The driving force is decreased slowly in space from supercritical to subcritical values, as indicated by the figure in the title. As was shown theoretically such ramps lead to a perfect selection of a single wavelength /1/. Experiments in Taylor-Couette flow /2,3/ with conical cylinders clearly confirm this vanishing of the wavelength band: A single wavelength is selected in the limit of an infinitely long ramp. It has been pointed out theoretically, however, that this wavelength is not unique /1,4/. In Rayleigh-Benard convection it depends on the combination of the geometrical (varying layer thickness) and thermal (varying temperature difference) part of the ramp. If so, different combinations at the left and right end of a convection cell could lead to different wavelengths. Such a situation is not stable, the patterns move from the small wavelength end to the long wavelength end driven by a phase diffusion process. This paper presents the experimental investigation of this phenomenon.

1. THEORY

1.1 Smooth Ramps in Rayleigh-Bénard Convection

Two-dimensional convection can be described by

$$R_o\,\partial_x T - \nabla^4\psi = 0, \qquad \left(\partial_t + (\partial_z\psi\,\partial_x - \partial_x\psi\,\partial_z)\right) T - \nabla^2 T = 0. \tag{1}$$

Here the Overbeck-Boussinesq-approximation and an infinite Prandtl number have been assumed and all quantities have been made dimensionless by using typical scales. The fluid is assumed to lie in the x-y-plane and the velocity $\underline{v}=(v_x,v_y)$ is given by the streamfunction ψ via $v_x=\partial_z\psi$ and $v_z=-\partial_x\psi$. The temperature is denoted by T and the Rayleigh number by R_o.

As indicated in the title we wish to analyze the convection pattern that arises for boundary conditions which depend smoothly and slowly on the x-coordinate. Therefore a slow spatial scale $X = \alpha x$ with $\alpha\ll 1$ is introduced. For simplicity the fluid is now assumed to be contained between an upper flat plate (z=0) and a lower plate at z=-G(X). Similarly, the temperature is taken to be constant (T=0) at z=0 and X-dependent at z=-G(X) (T=H(X)G(X)). Thus H(X) is the local temperature gradient in the non-convective state. To transform the region contained between the plates to a rectangle, new coordinates are introduced which are orthogonal to order $O(\alpha)$,

$$\zeta = z/G, \qquad \xi = x + \alpha\,(\zeta^2 - 1)\,G\,G'/2. \tag{2}$$

Here $G'=\partial_X G$. The boundary conditions now read

$$T = 0 \quad \text{at } \zeta = 0, \qquad T = H(X)\,G(X) \quad \text{at } \zeta = -1,$$

$$\psi = \partial_\zeta^2\psi = 0 \quad \text{at } \zeta = -1,\ 0. \tag{3}$$

For simplicity stress-free boundary conditions for ψ have been assumed. Rigid boundary conditions are expected to give qualitatively the same results. Note that with the coordinates (2) the usual free boundary conditions are in fact given by (3), which was not the case for the coordinates used in /4/.

How do we now obtain moving patterns? As mentioned above they result if in the *same* region two *different* wave numbers (or *disjoint* wave-number bands) are selected by suitable selection mechanisms. Therefore we briefly review wave-number selection by smooth ramps /1,4/.

Introducing θ via $T=HG(\theta-\zeta)$, θ and ψ are expanded in α,

$$\psi(\eta,X,\zeta,\tau) = \psi_o + \alpha\,\psi_1+\ldots, \qquad \theta(\eta,X,\zeta,\tau) = \theta_o + \alpha\,\theta_1 +\ldots \tag{4}$$

Both, ψ and θ are 2π-periodic in the phase η. In addition to the slow time τ a slow phase ϕ is introduced

$$\tau = \alpha^2 t, \qquad \eta = \alpha^{-1}\phi(X,\tau)/G. \tag{5}$$

Using $\partial_\xi=(q/G)\partial_\eta+\alpha\partial_X$ (1) is regained in $O(\alpha^0)$ with the local Rayleigh number

$R(X)=R_0 HG^4$ replacing R_0. Thus, to this order any local wave number $q(X)$ is possible as long as it stays within the band of stable solutions. Due to the singularity of the linearized operator $\mathcal{L}$ of (1) a solvability condition arises at order $O(\alpha)$, which is obtained by projecting the equations in $O(\alpha)$ onto the adjoint translational null mode (V_1^+, V_2^+) of $\mathcal{L}$ /4/,

$$\tau_0 \partial_\tau \phi = D \partial_X q + (B + E) \partial_X R/R + (C - 4B) \partial_X G/G. \tag{6}$$

Because the coefficients depend on $q=G\partial_\xi \eta = G\partial_X(\phi/G)$, (6) is a nonlinear diffusion equation for the phase ϕ, describing the effect of the ramped boundary conditions on the statics and slow dynamics of the periodic pattern. The coefficients are given by /5/

$$\tau_0 = \langle V_2^+ \partial_\eta \theta_0 \rangle,$$

$$D = -\langle V_1^+ \Big[R\partial_q \theta_0 - 4q(\partial_\zeta^2 + q^2\partial_\eta^2)\partial_\eta \partial_q \psi_0 - 2(\partial_\zeta^2 + 3q^2\partial_\eta^2)\partial_\eta \psi_0 \Big]$$

$$V_2^+ \Big[\partial_\zeta \psi_0 \partial_q \theta_0 - (\partial_\zeta \theta_0 - 1)\partial_q \psi_0 - (1 + 2q\partial_q)\partial_\eta \theta_0 \Big] \rangle,$$

$$B = -\langle V_1^+ R(\theta_0 - \zeta) + V_2^+ \Big[(\theta_0 - \zeta)\partial_\zeta \psi_0 - 2q\partial_\eta \theta_0 \Big] \rangle,$$

$$C = -\langle V_1^+ \Big[R(1 - \zeta\partial_\zeta)\theta_0 + 4q(\partial_\zeta^2 + q^2\partial_\eta^2)\partial_\eta \psi_0 \Big] + V_2^+ \Big[(\theta_0 - \zeta)\partial_\zeta \psi_0 - 2q\partial_\eta \theta_0 \Big] \rangle$$

$$E = -\langle V_1^+ \Big[R\,\partial_R^2 \theta_0 - 4q(\partial_\zeta^2 + q^2\partial_\eta^2)R\partial_R \partial_\eta \psi_0 \Big] +$$

$$V_2^+ \Big[(1 - \partial_\zeta \theta_0)R\partial_R \psi_0 + \partial_\zeta \psi_0\, R\partial_R \theta_0 - 2qR\partial_R \partial_\eta \theta_0 \Big] \rangle, \tag{7}$$

where $\langle ... \rangle$ denotes the average $\int_0^{2\pi} \int_{-1}^{0} ... d\zeta\, d\eta$. The expressions for B and C differ from those given in /4/ due to the different coordinate system. In addition, the fact has been used that the basic flow need not be calculated explicitly to order $O(\alpha)$.

The phase diffusion equation (6) shows that for ramps which become subcritical in some region the wave-number band collapses to a single wave number /1,4/. Consider now a system with a homogeneous part of length L which is connected to two different subcritical ramps at both ends. If these ramps select different wave numbers q_1 and q_2, say, then a wave-number gradient is established in the homogeneous region, which leads to phase diffusion (see (6) with R and G constant). This, however, never comes to an end, as the wave numbers at both ends are fixed by the ramps, and a moving pattern with velocity

$$v = D\,\partial_X q / q\tau_0 \tag{8}$$

is obtained. The only requirement for a system to support this dynamics is the existence of different ramps which select *different* wave numbers. For

Rayleigh-Benard convection this amounts to the condition that neither of the coefficients B+E and C-4B in (6) vanish identically. Close to threshold this requirement is in fact fulfilled as a calculation using the amplitude approximation shows /4,5/ (far from threshold and for rigid boundary conditions the coefficients have to be computed numerically, which has been done for pure thermal ramps only /6/). This can be seen in detail for the family of ramps given by /4/

$$\delta\ \partial_X G/G + (1 - \delta)\ \partial_X H/H = 0, \quad \delta = \text{const.} \tag{9}$$

The static phase diffusion equation can then be written as

$$(\varepsilon - 3p^2)\ \partial_\varepsilon p = 2\beta\ (\varepsilon - p^2) - p + 7p^2/\sqrt{48},$$

$$2\beta = (4b - c)\ \frac{1 - \delta}{4 - 5\delta} - b - 7/\sqrt{48}. \tag{10}$$

with

$$\varepsilon = (R - R_c)/R_c,\ R_c = 27\pi^4/4,\ p = \sqrt{8/3\pi^2}\ (q - q_c),\ q_c = \pi/\sqrt{2}.$$

$$B = - b\ (\varepsilon - p^2),\ b = 0.60, \quad C = - c\ (\varepsilon - p^2),\ c = 1.54, \tag{11}$$

The solutions to this equation with $p(\varepsilon=0)=0$ are given in fig. 1 for various values of β. It clearly shows that the selected wave number is *non-universal*, i.e. it depends on the ramp chosen. In fact, the slope of the selected wave number is given by $\partial_\varepsilon p=1/\beta$, which can be varied from $-\infty$ to ∞ by a suitable choice of δ.

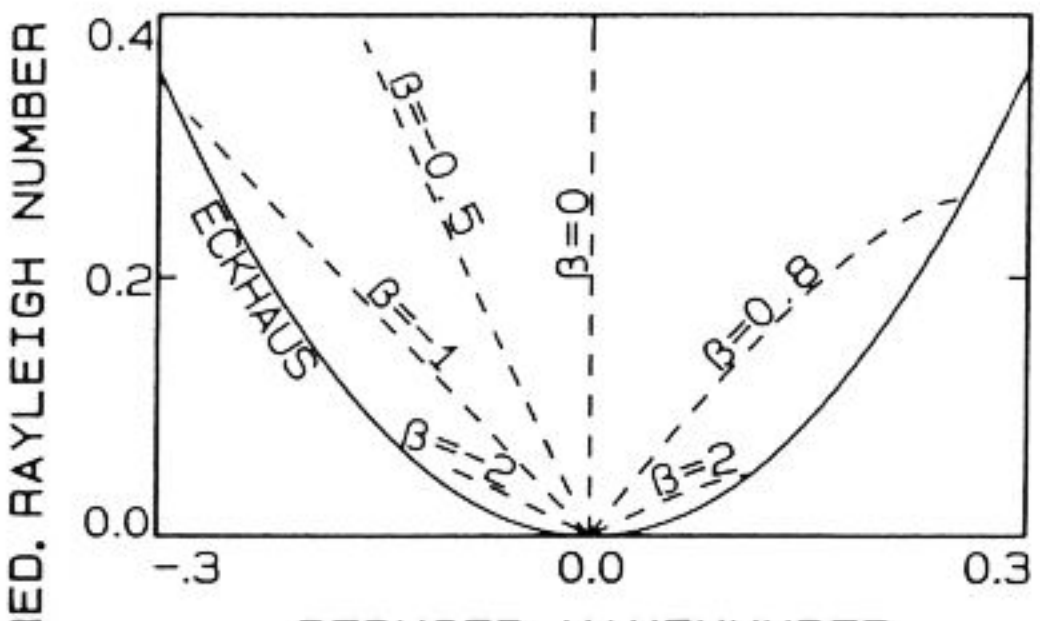

Fig. 1
Selected wave numbers for different ramps as given by (10)

Thus, according to this analysis moving patterns are possible in RB-convection and the threshold R_m for the motion coincides with the threshold R_c for the appearance of the pattern itself. The wave-number gradient $\partial_X q \cong (q_2 - q_1)/\alpha L$ and therefore also the velocity v grows linearly when increasing the Rayleigh number.

1.2 Imperfect Wave-number Selection by Pinning Ramps

How much of the analysis in sec.1 carries over to a real experiment where the basic requirement of this analysis, the perfectly smooth variation of the control parameters, is not really met? To clarify this it is useful to look at

the influence of the ramp on the basic state. This state is purely conductive for constant boundary conditions. For $\partial_X H \neq 0$, however, the ramp induces a large-scale convection with

$$v_X^B(\zeta,X) = -\alpha R\, \partial_X H\, (5\zeta^4 - 10\zeta^2 + 7/3)/120H + O(\alpha^2) \tag{12}$$

$$v_Z^B(\zeta,X) = \alpha^2\, \partial_X(R\, G\, \partial_X H/H)\, (\zeta^5 - 10\zeta^3/3 + 7\zeta/3)/120. \tag{13}$$

In particular, if H has a localized region with large curvature $\partial_X^2 H$, the vertical velocity v_z contains a peak-like term, which can lead to a pinning of the periodic convective pattern. In this section the influence of such *pinning centers* on wave-number selection is reviewed. It has been shown that in the usual set-ups they are the predominant cause for deviations from the perfect selection displayed in fig. 2 and lead to finite band widths Δq /7,5/. Because drifting of the pattern sets in only if the wave-number bands of different ramps do not overlap, its onset is expected to lie above the convection threshold ($R_m > R_c$).

For simplicity the analysis is demonstrated using an extension of the Swift-Hohenberg model /8/,

$$\partial_t \psi = \left[R - (\partial_X^2 + 1)^2\right]\psi - \psi^3 + G\,(1 - R + G^2), \tag{14}$$

where the additional term $G(1-R-G^2)$ has been introduced to obtain a non-trivial basic state

$$\psi^B = G + \alpha^2\, \frac{2q^2 \partial_X^2 G}{R - 1 - 3G^2} \tag{15}$$

similar to that in RB-convection (13). Again, the control parameters R and G are assumed to vary slowly and smoothly in space in two regions I and III. However, in region II, which separates I and III, they are allowed to vary more rapidly. As non-adiabatic effects are responsible for the wave-number bands a separate slow scale X *must not* be introduced. Instead, for R we require

$$\partial_X^n R = O(\alpha^n) \text{ in I and III}, \quad \partial_X^n R = O(\alpha) \text{ in II}, \quad \alpha \ll 1, \tag{16}$$

and analogously for G. This is, for instance, the case if two smooth ramps are joined in II with different slopes. In /7,5/ it is shown that the rapid variation in II leads to a matching condition for the wave numbers in the two phase diffusion regions I and III. Similarly to (6) it is obtained by projecting (14) in order $O(\alpha)$ with $\psi = \psi_0 + \alpha\psi_1 + ..$ onto the null mode. However, as ψ_1 is not 2π-periodic in the phase η in II, boundary terms appear, which are removed by a second integration over all of region II ($\eta_1 < \eta < \eta_2$). The resulting matching condition reads

$$D\left[q_2 - q_1 + \pi(\partial_\eta q_2 - \partial_\eta q_1)\right] = \frac{1}{q}\int_{\eta_1}^{\eta_2} d\eta \int_{\eta}^{\eta+2\pi} d\eta'\, \left[\rho(\eta'+\eta_0)\partial_\eta R + \gamma(\eta'+\eta_0)\partial_\eta G\right] \tag{17}$$

where $q_1=q(\eta_1)$ etc. and D, ρ and γ are functionals of ψ_o similar to A,B,C and E in (6) /7/. The crucial point of (17) is the dependence of the r.h.s on the phase η_o of the solution ψ_o relative to the ramp. This is illustrated in fig. 2 for a ramp of the form

$$R = R_1 - \Theta(-x)\,\Delta R'x, \quad G = G_1 - \Theta(-x)\,\Delta G'x, \tag{18}$$

with $\Theta(x)$ being the step function ($R_1=0.5$, $G_1=0.1$, $\Delta R'=-0.005$, $\Delta G'=0.0005$). This ramp becomes smoothly subcritical for $x\to-\infty$ and therefore yields perfect selection in region I ($q\cong q_c=1$). The wave number q in III is given by the matching condition (17) and therefore depends on η_o, the phase of ψ_o at x=0. The function $q(\eta_o)$ is 2π-periodic. Due to the harmonic content of ψ_o also higher harmonics are apparent (compare also with the experimental results for Taylor vortex flow, fig. 10 in /3/). Thus, although the wave number in I is perfectly selected, a wave-number band Δq arises in III through the η_o-dependent influence of the pinning center.

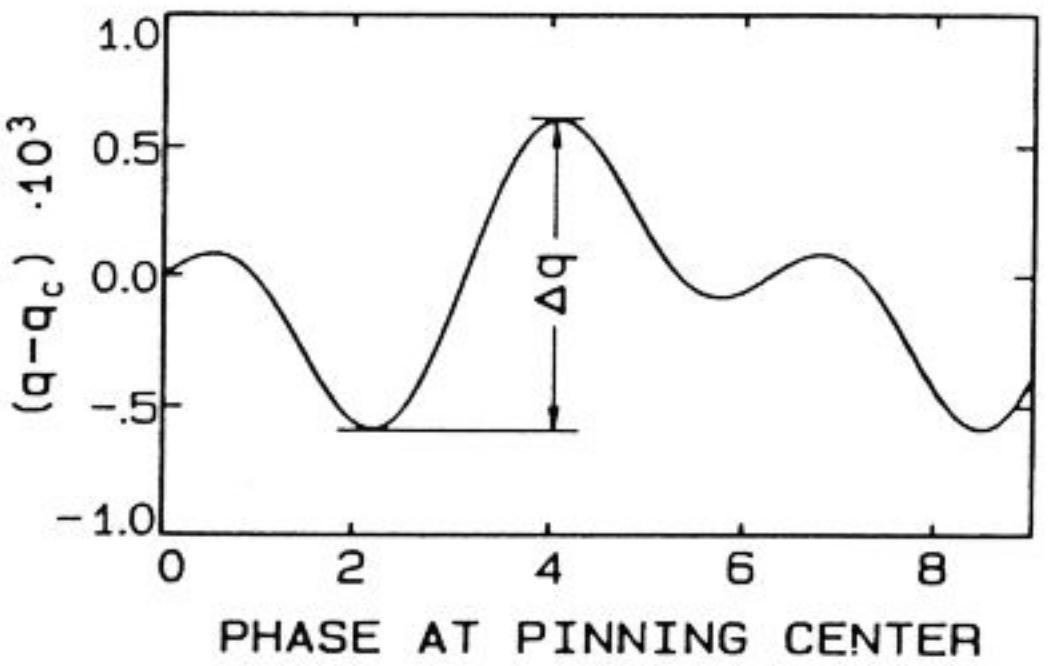

Fig. 2
Wave number q as a function of the phase η_o of ψ_o at x=0.
q is 2π-periodic.
Parameters:
$R_1=0.5$ $G_1=0.1$
$\Delta R'=-0.005$ $\Delta G'=0.0005$
(see (18))

A characteristic feature of wave-number bands produced by a pinning basic state is their dependence on the control parameter: close to threshold they *grow* with *decreasing* control parameter. This is shown in fig. 3, where the matching condition is compared with a numerical simulation of (14) ($\Delta R'=-0.001,-0.005$, $\Delta G'=0.0005$, $G_1=0.1$). This ("anomalous") behavior of the band width is also observed in Taylor vortex flow /2,3/. In these experiments a characteristic cross-over from the anomalous to the normal band is observed, which is also reproduced by the matching condition (17) when applied to a further extension of the model (14) /9/. Figure 3 shows very good agreement for larger $R-R_c$. For too small values of $R-R_c$ the validity of (17) breaks down due to the divergence of the correlation length at threshold.

To obtain moving patterns the wave-number bands of different ramps may not overlap. Therefore the pinning basic state will lead to a shift in the onset of motion to larger values of R as illustrated in fig. 5 below. As before, however, the velocity should still grow linearly from 0 when increasing R beyond onset. Experimentally, one is interested in minimizing the pinning in order to maximize the velocity. This is done by smoothing out the transition from the ramp to the homogeneous region. The matching condition shows that this very efficiently reduces the band width. Figure 4 gives the result for rounded ramps of the form

$$R = \tfrac{1}{2}R'\left[x - d\ \ell n(2\cosh\tfrac{x}{d})\right] + R_1, \qquad \text{i.e. } \partial_x R = \tfrac{1}{2}R'(1 - \tanh\tfrac{x}{d}), \tag{19}$$

with G=0, R_1=1, R'=0.1. These ramps lead in amplitude approximation to

$$\Delta q = \left|\tfrac{1}{4}R'\right| \frac{\pi d\ \sinh(\pi d)}{\cosh(2\pi d)-1}\ . \tag{20}$$

Thus, already a rounding over a quarter of a wavelength (d=1.5) reduces the band width by a factor of 6. A similar result was obtained in a numerical simulation of Taylor-Couette flow /10/.

Figure 5 summarizes the results of the theoretical analysis qualitatively. In RB-convection close to threshold any wave number in the stable band can be selected by a suitable ramp. For realistic ramps with a finite length and with pinning centers each selection curve is expanded to an anomalous band, which

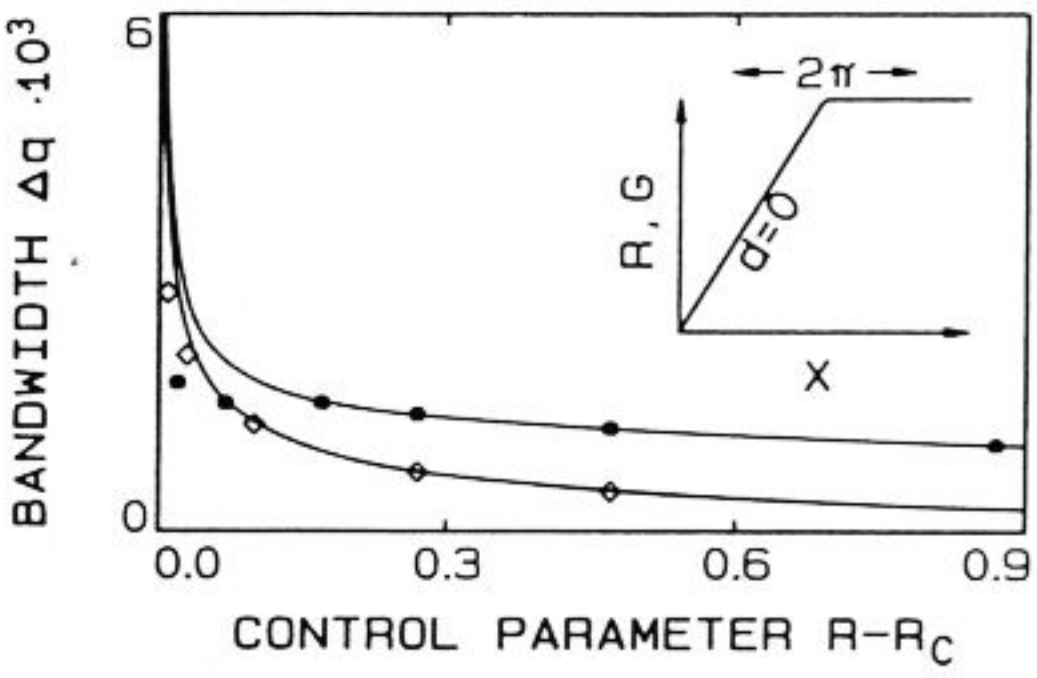

Fig. 3
Wave-number band for ramp with discontinuous slope.

The lines represent (17). The symbols are obtained by a numerical simulation of the model (14).
Parameters:
$\Delta G'=0.0005$, $G_1=0.1$
solid circles: $\Delta R'=-0.005$
open diamonds: $\Delta R'=-0.001$

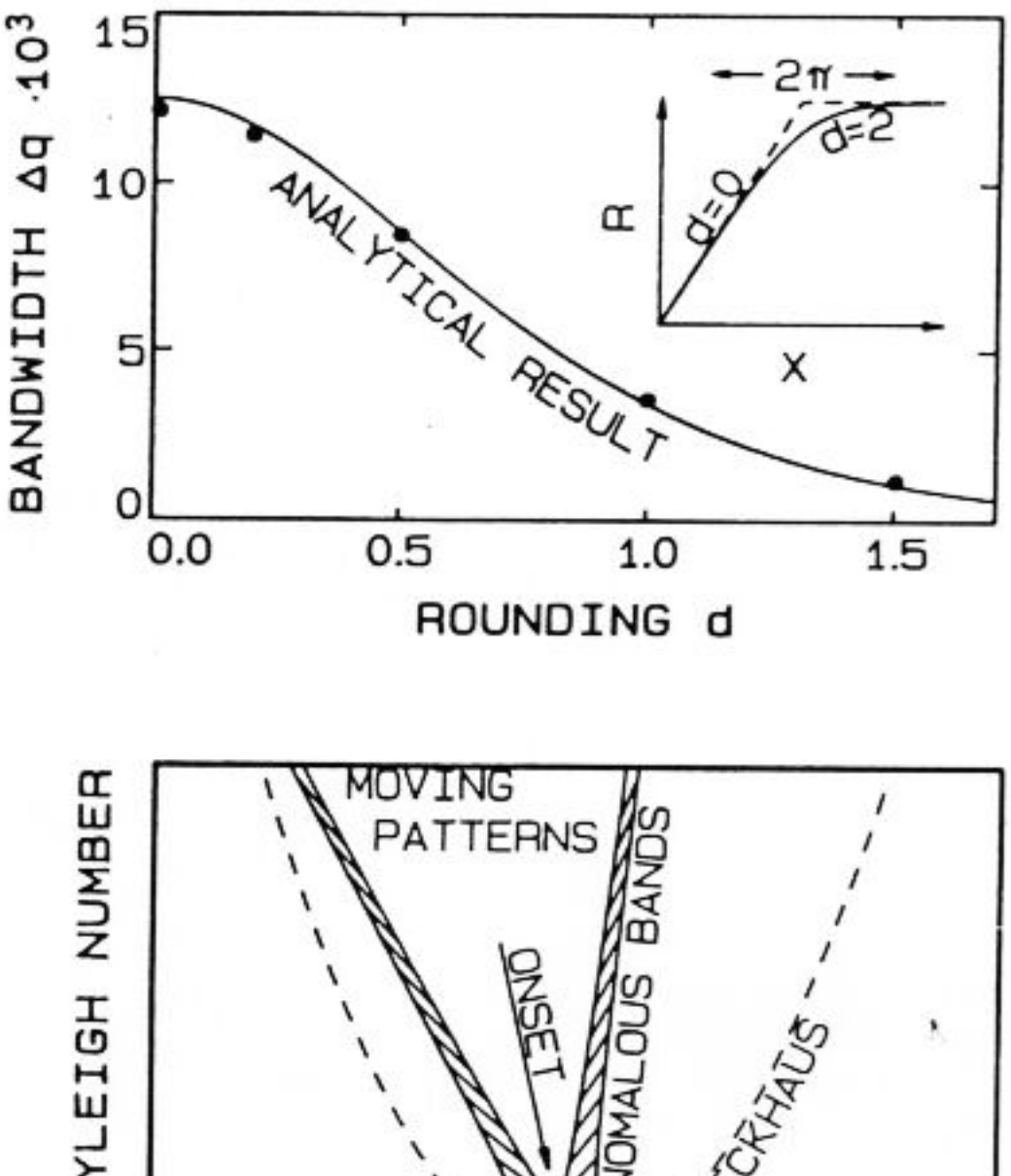

Fig. 4
Wave-number band for ramp with continuous slope

The solid circles are obtained by numerical integration of model (14). The line represents (20).
Parameters:
G=0, R_1=1, R'=0.1

Fig. 5
Schematic explanation for the existence of moving patterns. Dashed regions indicate the bands selected by the two different ramps

widens close to the convection threshold R_c. Therefore the bands will overlap there. The patterns will start to move above a threshold $R_m > R_c$ where this overlap ceases to exist. The exact position of this critical point thus depends sensitively on the smoothness of the ramps. The velocity v increases linearly with R close to R_m.

2. EXPERIMENTAL RESULTS

Governed by the theoretical arguments summarized above, a convection cell was designed in order to observe the predicted drifting convection patterns. The shape of the convection box is cut out of a copper plate of 1.5mm thickness. The height in the middle of the cell is 3mm over a length of 18mm, thus allowing at least 3 pairs of convection rolls within this bulk part. The subcritical ramps to the left and right of this part are obtained by cutting a parabolic curve out of the copper as indicated in fig. 6. The height of the cell in the ramps is decreased from 3mm to 1mm over a distance of 26mm. The cell is heated from below by means of constant electrical power. The top of the cell is attached to an aluminium block regulated to a constant temperature (20°C) by means of a water circuit. Cyclohexan was used as the working fluid. Note that this design leads to a combination of a geometrical and a thermal ramp because the copper at both sides forms a thermal short-circuit. This thermal ramp can be influenced on the right hand side by an additional heater.

The method used for the flow visualisation is the shadowgraph technique: Density gradients in the fluid caused by temperature gradients lead to light intensity modulations. This light intensity is measured with a photodiode which can be moved parallel to the convection cell under computer control by a stepping motor.

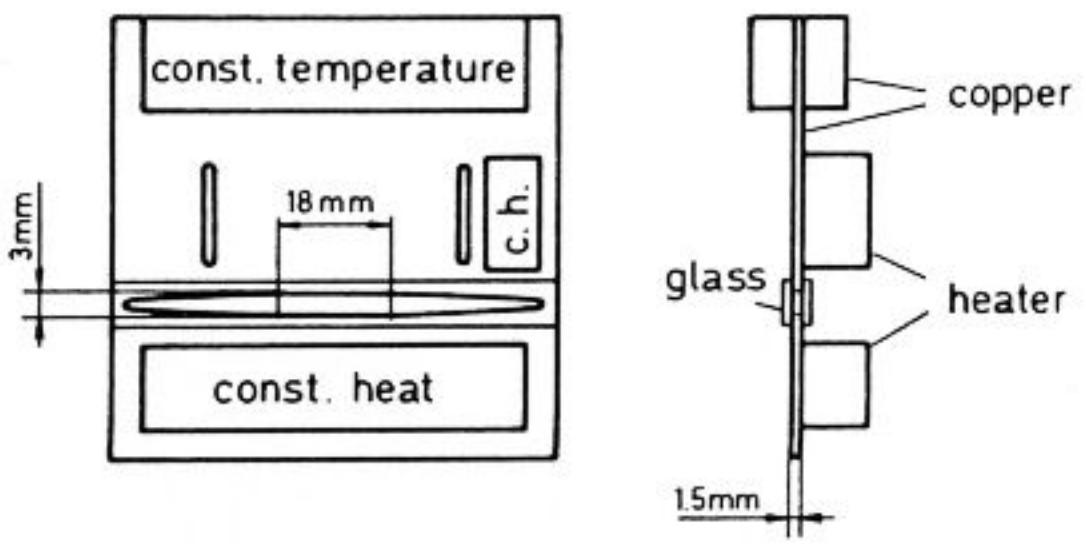

Fig. 6
Convection cell
(not to scale)

The height of the convection cell is 3mm, the length of its bulk part 18mm. Note the additional heater on the right hand side (c.h.).

Figure 7 shows scans of the light intensity at various temperature differences measured in the bulk part of the cell (position 0 corresponds to the middle of the cell) The scan at 2.5K temperature difference shows no modulation, this difference is clearly below the convection threshold (modulations of the light intensity caused by spatial inhomogenities of the light source are taken away by image division). The measurement at 9.9K is clearly above the convection threshold – intensity peaks are visible. These are caused by the colder (sinking) parts of the fluid. Their position is not constant, but a function of the temperature difference. The peaks move to the right when increasing this difference, but they tend to come back to their original position when decreasing this difference, as indicated by the dashed lines. The difference between the solid and dashed curves is expected to go to zero when increasing the waiting time between successive temperature steps.

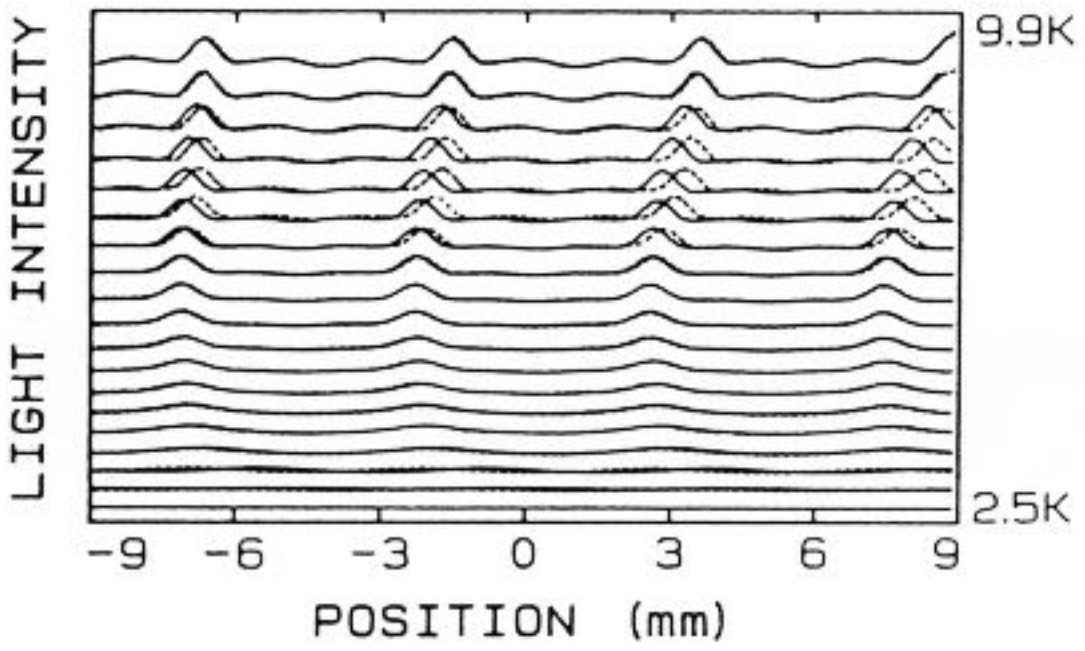

Fig. 7
Intensity profiles for various temperature differences in the range between 2.5K and 9.9K.

Intensity peaks (caustics) correspond to the location of cold sinking fluid.

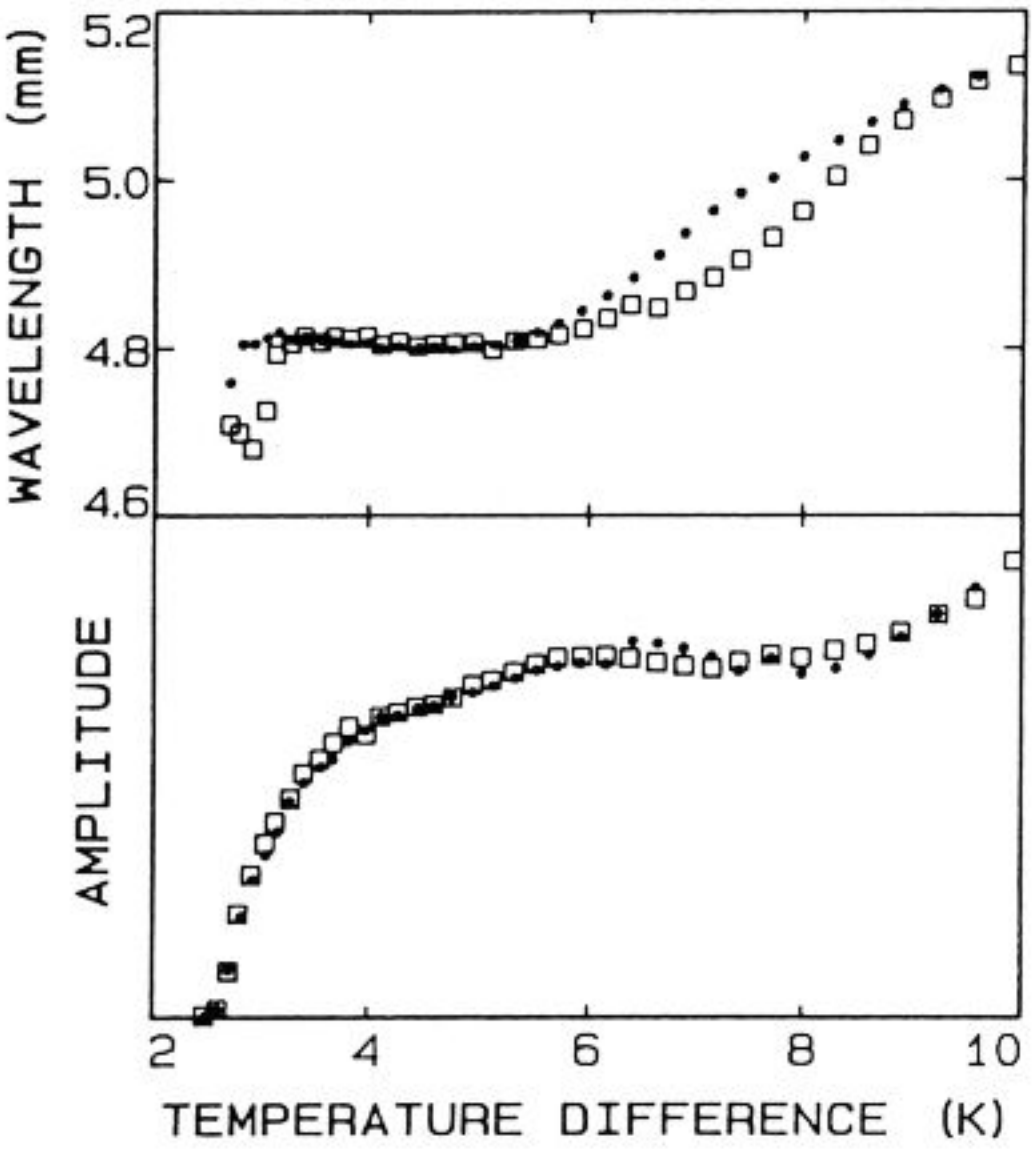

Fig. 8
Amplitude of the light intensity modulation and wavelength of the convection patterns as a function of the temperature difference

By spectral analysis the amplitude of the light intensity modulation and the wavelength of the convection pattern can be extracted from the profiles shown in the above figure. The amplitude is expected to be proportional to the temperature modulations in the fluid in the limit of small modulations, i.e. close to the convection threshold. The lower part of fig. 8 shows the result. Because the temperature modulation is known to grow according to a square-root law, the same would be expected for the intensity modulation in the neighborhood of the threshold. Measurements like this allow a determination of the critical temperature difference for the onset of convection (2.63K). The upper part of fig. 8 shows the wavelength of the convection patterns. Here a difference between data points obtained when increasing the temperature (open squares) and decreasing the temperature (solid circles) is observed. This indicates that the waiting time between consecutive data points (30 minutes) is long enough for the amplitude of the convection to reach its equilibrium value, but too short for the phase diffusion process to adjust the length and position of the convection pattern. Like in the previous figure, the difference between the two curves is expected to go to zero for a longer waiting time. The important feature of figure 8 is the smooth variation of the wavelength. This is made possible by the ramps and unlike the discontinuous jumps of the wavelength observed in convection boxes with sharp corners.

The measurements shown in figs. 7,8 are done without the side wall heating. No moving patterns are observed in that case, except for the transients when reaching the equilibrium position. If the symmetry of the two ramps is broken by means of the additional heater, drifting convection patterns become possible. This is demonstrated in fig. 9. The heater is located at the left end (negative positions). Thus the temperature difference is already subritical at a position of −15mm, while on the other end the critical position seems to be close to +30mm. The profiles are taken within time intervals of 15 minutes and plotted on top of each other. The movement of the patterns from the right to the left is clearly visible.

As indicated by fig. 9 the velocity of the moving patterns is not constant but rather a periodic function of time. One way to measure the mean velocity is to locate a photodiode at a fixed position and to measure the frequency of the time-periodic intensity modulations. These frequencies are plotted in fig. 10 as a function of the reduced temperature difference ε. The onset of motion is located at ε=0.4, i.e. well above the onset of convection. The frequency goes down to small values at this point. More measurements are needed to evaluate the detailed structure of the frequency curve at this point. The data presented are consistent with the statement that the frequency would go to zero monotonically when approaching R_m. Measurements close to this point obviously become time-consuming - the lowest measured frequency corresponds to a period of 20 hours.

Increasing the temperature difference leads to an increase of the travelling speed of the convection patterns. If ε is too large, however, this movement has to come to an end because the whole cell is supercritical then. A discussion of this second transition was not attempted here. It would presumably require an inclusion of the lateral boundary conditions.

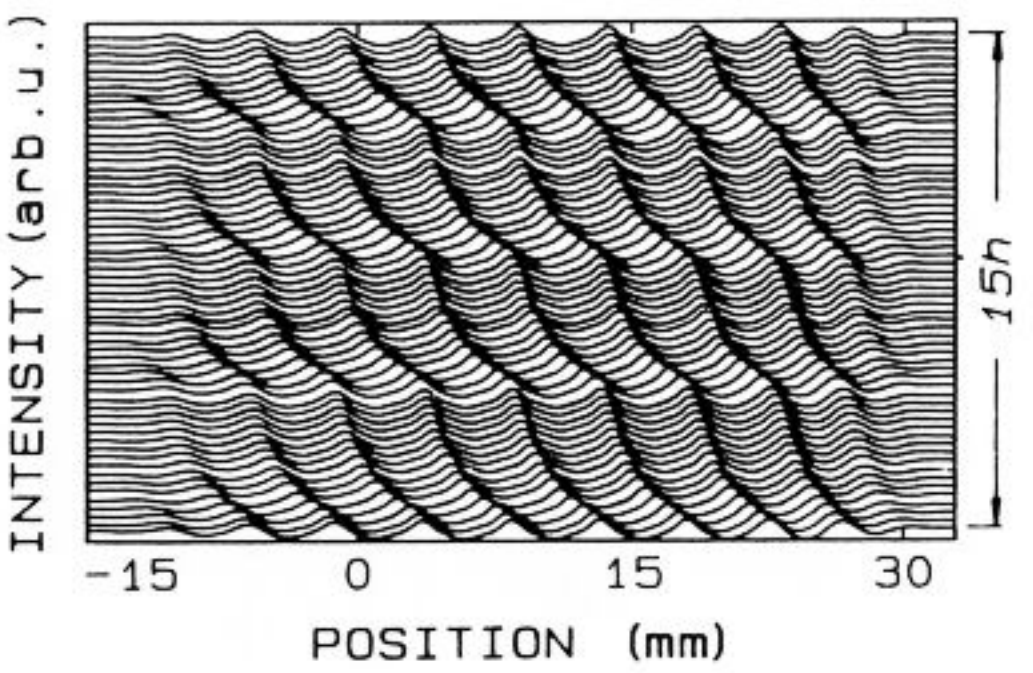

Fig. 9
Light intensity scans at different times. The time interval between two scans is 15 minutes

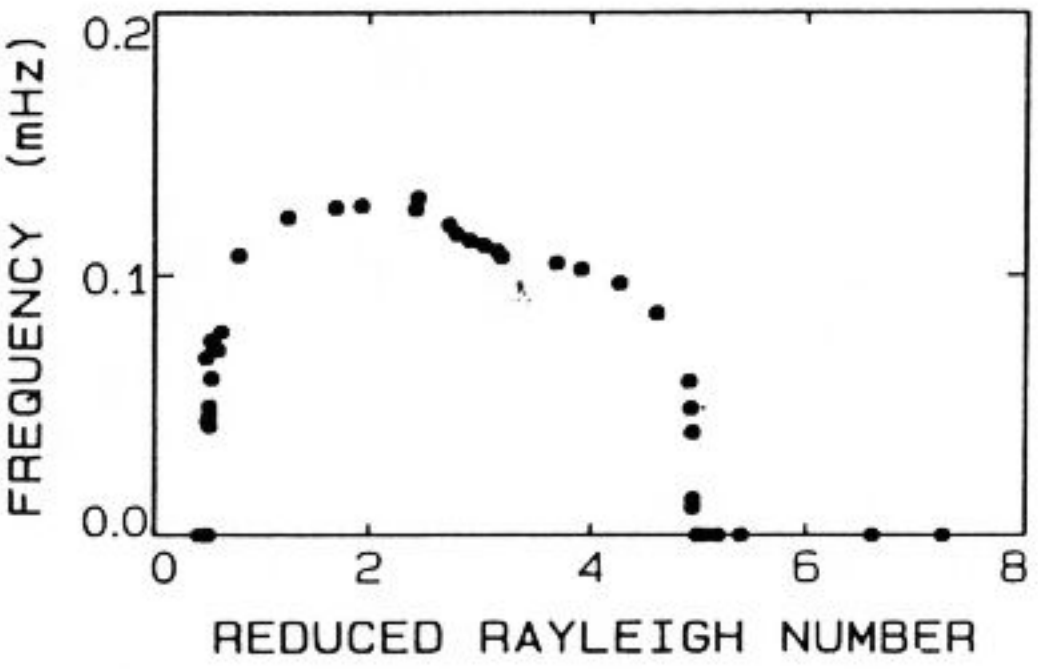

Fig. 10
Frequency of the light intensity modulations measured by a stationary photodiode

The periodic signal is caused by the drifting convection patterns. Its frequency is proportional to the velocity.

In this paper drifting patterns have been discussed using phase diffusion theory for the wavelength selection by ramps. This theory explains the experimental observations, provided that the effect of pinning centers is taken into account.

Acknowledgement

The theoretical work by H.R., which is part of his Ph.D. thesis, has been done under the supervision of L. Kramer. H.R. also thanks H.-G. Paap for his contributions to the choice of coordinates. The experimental work of I.R. was started following suggestions of F.H. Busse and has been done with the help of E. Bodenschatz, B. Winkler and S. Rasenat.

References

1. L. Kramer, E. Ben-Jacob, H. Brand, M.C. Cross:
   Phys. Rev. Lett. 49, 1891 (1982)
2. D.S. Cannell, M.A. Dominguez-Lerma, G. Ahlers:
   Phys. Rev. Lett. 50, 1365 (1983)
3. M.A. Dominguez-Lerma, D.S. Cannell, G. Ahlers:
   Phys. Rev. A34, 4956 (1986)
4. L. Kramer, H. Riecke: Z. Phys. B59, 245 (1985)
5. H. Riecke: Ph.D. thesis, Universität Bayreuth (1986)
6. J.C. Buell, I. Catton: preprint (1985)
7. H. Riecke: Europhys. Lett. 2, 1 (1986)
8. J. Swift, P.C. Hohenberg: Phys. Rev. A15, 319 (1977)
9. H. Riecke: to be published
10. M. Lücke: unpublished